Four Important Onset Pressures for Mutual Interactions between Each of Three Crude Oils and CO_2[†]

Xiaoqi Wang, Shiyang Zhang, and Yongan Gu*

Petroleum Technology Research Centre (PTRC), Petroleum Systems Engineering, Faculty of Engineering and Applied Science, University of Regina, Regina, Saskatchewan S4S 0A2, Canada

In this paper, mutual interactions between each of three different crude oils and CO_2 are experimentally studied. Three crude oils include two light crude oils and one medium crude oil. First, a series of saturation tests are conducted to determine the onset pressure of asphaltene precipitation for each crude oil−CO_2 system. Second, the equilibrium interfacial tension (IFT) between each crude oil and CO_2 is measured as a function of the equilibrium pressure. The so-called minimum miscibility pressure (MMP) of each crude oil−CO_2 system is determined by applying the vanishing interfacial tension (VIT) technique. Third, the oil-swelling effect and initial strong light-components extraction are observed during the IFT measurements. It is found that the onset pressure of asphaltene precipitation is lower if the asphaltene content of the crude oil is higher. It is also found that the measured equilibrium IFT is reduced almost linearly with the equilibrium pressure in three distinct pressure ranges for the two light crude oil−CO_2 systems and in two different pressure ranges for the medium crude oil−CO_2 system. The determined MMP is higher if the crude oil is heavier. The oil-swelling effect occurs at a low pressure, but the initial strong light-components extraction becomes dominant at a high pressure.

Introduction

Enhanced oil recovery (EOR) becomes increasingly important to the petroleum industry. After the primary and secondary recovery, a typical residual oil saturation in a light or medium oil reservoir is still in the range of (50 to 60) % of the original-oil-in-place (OOIP). Thus, the EOR processes contribute significantly to the overall oil production.[1] Among all the EOR methods developed for the light and medium oil reservoirs, carbon dioxide (CO_2) flooding has been successful to a large extent under some favorable reservoir conditions.[2] It is worthwhile to emphasize that the CO_2 EOR method not only effectively enhances oil recovery by (12 to 25) % of the OOIP[3] but also considerably reduces greenhouse gas emissions.[4]

Asphaltene precipitation is a major technical concern in CO_2 flooding and has a significant effect on its EOR.[5] It may occur if a sufficient amount of CO_2 is dissolved into the crude oil. The precipitated asphaltenes may be deposited onto the sand grains and thus left in the reservoir. In this case, asphaltene deposition can cause reservoir plugging and wettability alteration, which can greatly reduce the oil recovery. The produced crude oil is in situ deasphalted and becomes lighter and less viscous in comparison with the original crude oil.[6] On the other hand, if the precipitated asphaltenes are produced with the deasphalted oil from the reservoir formation, they can severely clog the downhole wellbore and cause surface treating problems.[7] Hence, it is important to determine the onset pressure of asphaltene precipitation for a given crude oil−CO_2 system.

It has been found that CO_2 EOR is largely controlled by the interfacial interactions between the injected CO_2 and reservoir oil, brines,[8] and rocks. These mutual interactions determine the overall performance of CO_2 flooding to a large extent. For example, a low interfacial tension (IFT) between the crude oil and CO_2 leads to a low residual oil saturation in the CO_2 flooding process. In addition, CO_2 is usually not miscible with a reservoir crude oil at the first contact but can develop the so-called dynamic miscibility with it through multiple contacts,[9] which is also referred to as the multicontact miscibility. In the latter case, mutual miscibility is achieved through two-way interfacial mass transfer between the crude oil and CO_2.[10] This fact indicates that the interfacial mass transfer plays an important role in developing the dynamic miscibility. The foremost technical issue in optimization or design of a CO_2 flooding project is to determine the minimum miscibility pressure (MMP) between a crude oil and CO_2.[11] The MMP of a given crude oil−CO_2 system is defined as the minimum pressure at which CO_2 can achieve the multicontact miscibility with the crude oil.[9] Among the existing experimental methods for determining the MMP, the slim-tube method is the most commonly used technique, and the rising-bubble apparatus (RBA) is recognized as a cheaper and faster alternative to the slim-tube method. Recently, a new experimental approach, named the vanishing interfacial tension (VIT) technique, has been developed and utilized to determine the miscibility conditions of different crude oil−CO_2 systems.[12,13] It is based on the concept that the IFT between the crude oil and a solvent must approach zero when these two phases become miscible. Because the smallest amounts of oil and time are required, the VIT technique is the cheapest and fastest among the three experimental methods for determining the MMP. Its reliability and accuracy have been discussed in the literature.[12−15]

In the previous studies,[14,15] a medium crude oil−CO_2 system was tested in a see-through windowed high-pressure cell by using the VIT technique. The following increasing-pressure order was established among onset pressure (P_{asp}) of asphaltene precipitation, the onset pressure (P_{ext}) of the initial strong light-

[†] Part of the "Sir John S. Rowlinson Festschrift".

* Corresponding author. Tel.: 1-306-585-4630. Fax: 1-306-585-4855. E-mail: peter.gu@uregina.ca.

10.1021/je1005664
Published on Web 08/26/2010

Table 1. Physical and Chemical Properties of Three Crude Oil Samples, Including Density ρ_{oil}, Viscosity μ_{oil}, API Gravity, Molecular Weight M_{oil}, and Mass Fraction of Asphaltene Content w_{asp}

oilfield	Joffre Viking	Pembina Cardium	Weyburn
CO_2 EOR stage	intermediate	early	intermediate
crude oil	light	light	medium
ρ_{oil}(300.15 K)/(g·cm^{-3})	0.815	0.835	0.912
μ_{oil}(300.15 K)/(mPa·s)	3.2	5.5	24.4
API gravity/°API	41.7	37.5	23.3
M_{oil}/(g·mol^{-1})	185.3	212.1	322.0
w_{asp}	0.0010	0.0026	0.0630

components extraction, the so-called minimum IFT pressure (P_{IFT}), the so-called maximum CO_2 EOR pressure (P_{EOR}), and the MMP: $P_{asp} < P_{ext} < P_{IFT} \approx P_{EOR} <$ MMP. In particular, the MMP determined by applying the VIT technique was found to be slightly higher than but close to P_{IFT} from a series of the equilibrium IFT measurements[14] and P_{EOR} through a series of CO_2 EOR coreflood tests.[15] However, the order of these important onset pressures and the related physical phenomena observed during the IFT measurements has been neither systematically studied nor verified for other different crude oil−CO_2 systems.

In this paper, an experimental approach is adopted to study the mutual interactions between each of three different light/medium crude oils and CO_2 under various pressures. In particular, the order for the above-mentioned three important onset pressures (i.e., P_{asp}, P_{ext}, and MMP) and the miscibility pressure (P_{max}) between the heavy components of a crude oil and CO_2 is determined for each crude oil−CO_2 system. Also, several major physical phenomena are analyzed and compared. More specifically, first, the onset pressure (P_{asp}) of asphaltene precipitation is determined for each crude oil−CO_2 system, and the morphology of the precipitated asphaltenes is observed and described. Second, the IFTs between each crude oil and CO_2 are measured at different equilibrium pressures and $T = 300.15$ K, and the MMP for each crude oil−CO_2 system is determined by applying the VIT technique. Lastly, the oil-swelling effect and initial strong light-components extraction from the crude oil to CO_2 are visualized during the IFT measurements. The onset pressure (P_{ext}) of the initial strong light-components extraction for each crude oil−CO_2 system is noted as well.

Experimental Section

Materials. Three crude oil samples were collected from Joffre Viking, Pembina Cardium, and Weyburn oilfields, Canada, respectively. Some major physicochemical properties of each cleaned crude oil are listed in Table 1. It is worthwhile to note that Pembina Cardium oilfield is currently in the early CO_2 EOR process, whereas Joffre Viking and Weyburn oilfields have been under CO_2 flooding since 1984 and 2000, respectively. The crude oils from Joffre Viking and Pembina Cardium oilfields are categorized as light oils, whereas the crude oil from Weyburn oilfield is considered as a medium oil based on the measured density or API value of each oil sample. A freezing-point osmometer (model 5009, Precision Systems Inc., USA) was used to measure the apparent molecular weights of the three original crude oils. The asphaltene content (pentane insoluble) of each original crude oil was measured by using the standard ASTM D2007-03 method.[16] The mole fraction purity of carbon dioxide (Praxair, Canada) used in this study was 0.99998. The densities of CO_2 at different pressures and $T = 300.15$ K were calculated by using the CMG Winprop module (Version 2008.10, Computer Modelling Group Limited, Canada) with Peng−Robinson equation of state (EOS).[17]

The compositional analysis result of each original crude oil sample was obtained by using the standard ASTM D86[18] and is plotted in Figure 1. It is found from this figure that Joffre Viking crude oil has the largest amount of light components, which is followed by Pembina Cardium crude oil, whereas Weyburn crude oil has the least amount of light components. The measured data in Table 1 and Figure 1 show that by comparison Joffre Viking light crude oil is the lightest, Pembina Cardium light crude oil is in the middle, and Weyburn medium crude oil is the heaviest among the three crude oils.

Asphaltene Content Measurement. The asphaltenes were precipitated from an original crude oil by using the standard ASTM D2007-03 method.[16] More specifically, one volume of the original crude oil was mixed with forty volumes of liquid pentane, which was used as a precipitant. The crude oil−precipitant mixture was agitated by using a magnetic stirrer (SP46925, Barnstead/Thermolyne Corporation, USA) for 12 h. Two 2 μm pore size filter papers were weighed by using an electric balance (AG204, Mettler Toledo, Switzerland) before they were used to filter the crude oil−precipitant mixture. The filter cake, which was primarily composed of the precipitated asphaltenes, was kept rinsing with pentane until the precipitant remained colorless after it passed through the filter papers. The filter papers with the precipitated asphaltenes were slowly dried at $T = 300.15$ K in an oven (650-58, Fisher Scientific, Canada) until their total weight did not change from the reading of the electric balance. With the measured weight change of the filter papers before and after filtration, the asphaltene content (pentane insoluble) of the original crude oil sample was determined accordingly.

Onset of Asphaltene Precipitation. In this study, a visual method is applied to measure the onset pressure of asphaltene precipitation. Figure 2 shows the schematic diagram of the experimental setup used to determine the onset pressure of asphaltene precipitation for a given original crude oil−CO_2 system. The major component of this experimental setup was a specially designed see-through windowed high-pressure saturation cell with a total volume of 310 cm^3. In this saturation cell, a thick stainless steel plate was machined and placed between two transparent acrylic plates to form a rectangular cavity (30.48 × 5.08 × 1.91 cm^3). The maximum operating pressure of this saturation cell is equal to 7.0 MPa at $T = 300.15$ K. A light source and a glass diffuser (240-341, Dyna-Lume, USA) were placed beneath the saturation cell to provide sufficient and uniform illumination for CO_2-saturated oil layer. A microscope camera (MZ6, Leica, Germany) was positioned above the saturation cell to capture the digital image of a CO_2-saturated oil layer inside the saturation cell at any time. The digital images of the CO_2-saturated oil layer under different equilibrium pressures were acquired in tagged image file (TIF) format by using a digital frame grabber (Ultra II, Coreco Imaging, Canada) and stored in a DELL desktop computer.

Prior to each saturation test, the saturation cell was cleaned with kerosene, then flushed with nitrogen, and finally vacuumed. The high-pressure saturation cell was pressurized with CO_2 to $P = 3.0$ MPa at the beginning. Then 5 cm^3 of the crude oil was introduced into the saturation cell by using a programmable syringe pump (100DX, ISCO Inc., USA). This small amount of the crude oil was chosen and injected into the saturation cell so that a thin oil layer ($\approx$ 0.032 cm) was formed on the lower acrylic window of the saturation cell and thus could be sufficiently illuminated by using the light source. The CO_2-saturated oil layer was observed through the acrylic windows of the saturation cell by using the microscope camera. The personal computer was connected to the microscope camera and

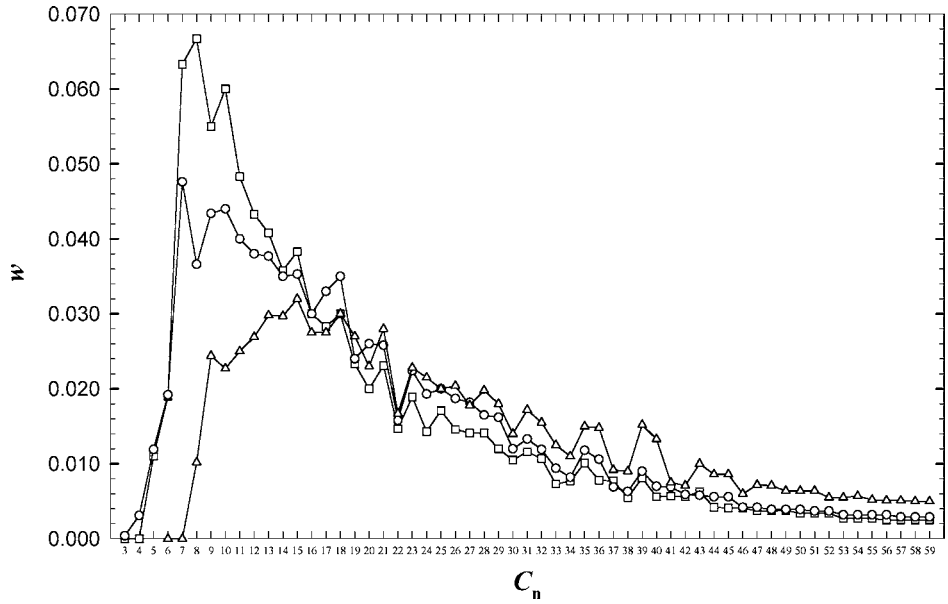

Figure 1. Compositional analysis results for three original crude oil samples, where w is mass fraction and C_n denotes carbon number. □, Joffre Viking with $w(C_{60+}) = 0.0819$; ○, Pembina Cardium with $w(C_{60+}) = 0.1021$; △, Weyburn with $w(C_{60+}) = 0.2094$.

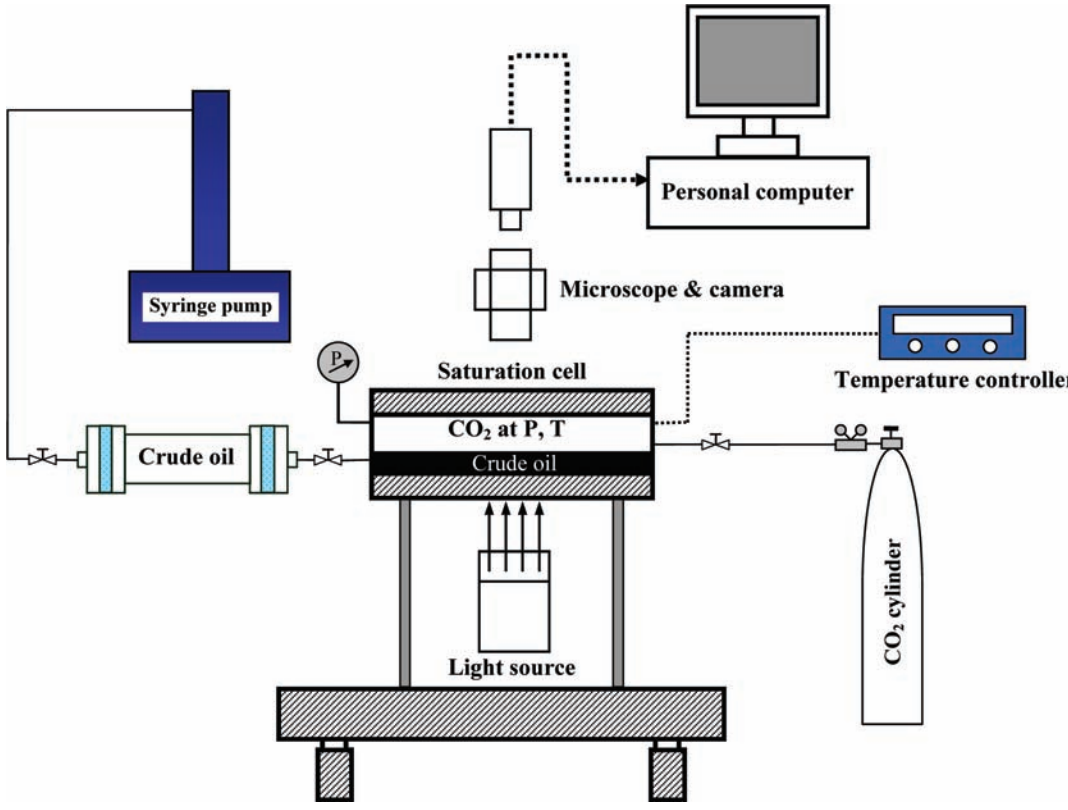

Figure 2. Block diagram of the experimental setup used for determining the onset pressure of the asphaltene precipitation from a crude oil−CO_2 system.

used to acquire the digital image of the CO_2-saturated oil layer at any time. In this way, any asphaltene deposits on the lower acrylic window at a proper saturation pressure could be clearly observed. In particular, the corresponding onset pressure of the asphaltene precipitation from the CO_2-saturated oil layer was noted.

IFT Measurement. Figure 3 shows the schematic diagram of the experimental setup used for measuring the equilibrium IFT between the crude oil and CO_2 by applying the axisymmetric drop shape analysis (ADSA) technique for the pendant drop case.[19] The major component of this experimental setup was a see-through windowed high-pressure cell (IFT-10, Temco, USA). A stainless steel syringe needle was installed at the top of the pressure cell and used to form a pendant oil drop. The crude oil was introduced from the original crude oil sample cylinder (500-10-P-316-2, DBR, Canada) to the syringe needle by using the programmable syringe pump. The light source and the glass diffuser were used to provide uniform illumination for the pendant oil drop. The microscope camera was used to capture the sequential digital images of the dynamic pendant oil drop inside the pressure cell at different times. The high-pressure cell was positioned horizontally between the light source and the microscope camera. The entire ADSA system and high-pressure cell were placed on a vibration-free table

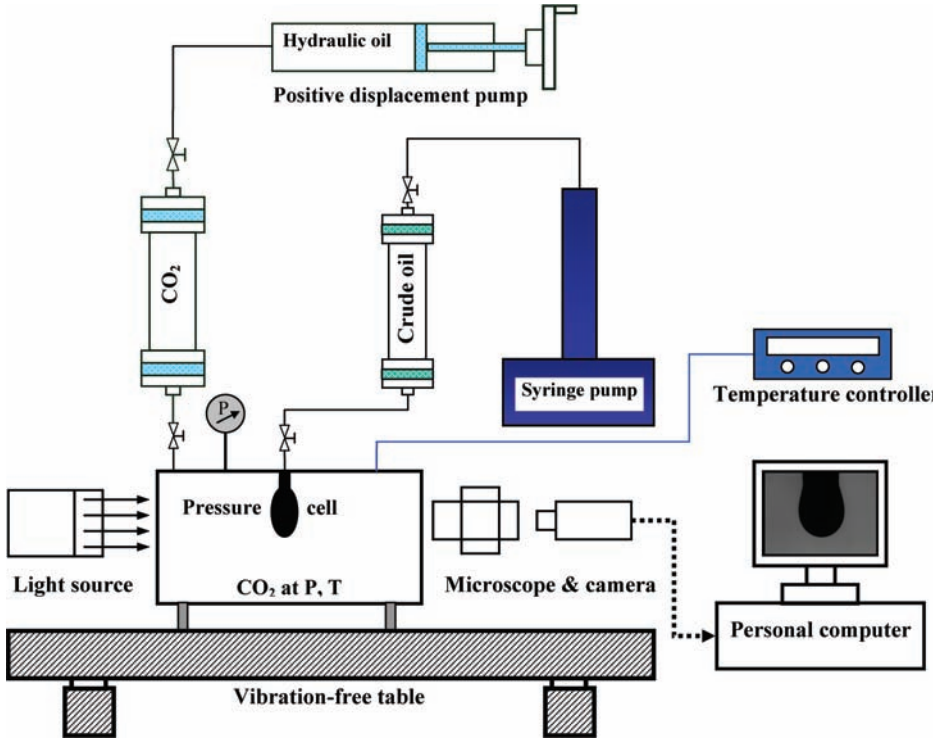

Figure 3. Block diagram of the experimental setup used for measuring the equilibrium interfacial tension (IFT) between the crude oil and CO_2 by applying the axisymmetric drop shape analysis (ADSA) technique for the pendant drop case.

(RS4000, Newport, USA). The digital image of the dynamic pendant oil drop at any time was acquired in a TIF file by using the digital frame grabber and stored in the DELL desktop computer.

The high-pressure cell was first filled with CO_2 at a prespecified pressure and a constant temperature. After the pressure and temperature inside the pressure cell reached their stable values, the crude oil was introduced from the original crude oil sample cylinder to the high-pressure cell to form a pendant oil drop at the tip of the syringe needle. Once a well-shaped pendant oil drop was formed, the sequential digital images of the dynamic pendant oil drop at different times were acquired and stored automatically in the personal computer. Then, the ADSA program for the pendant drop case was executed to determine the dynamic IFT of the dynamic pendant oil drop. The IFT measurement was repeated for at least three different pendant oil drops to ensure satisfactory repeatability at each prespecified pressure and constant temperature. Only the average value of the equilibrium IFTs of three repeated IFT measurements at each equilibrium pressure is presented in this study. Then the VIT technique was applied to determine the MMP of each crude oil−CO_2 system from the measured average equilibrium IFT versus equilibrium pressure data at $T = 300.15$ K.

Oil-Swelling Effect and Light-Components Extraction. The see-through windowed high-pressure cell used in the IFT measurements makes it possible to visualize the interfacial interactions between the crude oil and CO_2 under different equilibrium pressures up to 68 MPa. It was found that, at low equilibrium pressures, there was an initial oil-swelling process, which was followed by the subsequent weak light-components extraction process. The former process was revealed by volume increase of the dynamic pendant oil drop as CO_2 was gradually dissolved into the oil phase. The latter process was characterized by its volume reduction as the light components of the pendant oil drop were slowly extracted into the CO_2 phase. These findings show that, at a low equilibrium pressure, the initial CO_2 dissolution into the oil phase is dominant,[20] and then the subsequent weak light-components extraction from the oil phase to the CO_2 phase becomes pronounced,[14] though in fact the two-way mass transfer occurs at all times across the interface between the oil and CO_2 phases.[21]

At a high equilibrium pressure, the initial strong light-components extraction was observed and considered as an important physical phenomenon, in which the light components of the crude oil were rapidly extracted from the pendant oil drop to CO_2 phase at the beginning. Then again, the subsequent weak light-components extraction occurred. This indicates that the mass transfer from the oil phase to the CO_2 phase (i.e., an extraction or vaporizing process) is always dominant after the crude oil contacts CO_2 at a high equilibrium pressure. On the basis of these observations, the onset pressure of the initial strong light-components extraction was determined accordingly.

Results and Discussion

The compositional analysis results for the three original crude oils shown in Figure 1 indicate large differences among their carbon number distributions, which not only definitely lead to their rather different physical and chemical properties given in Table 1 but also considerably affect their mutual interactions with CO_2 at different pressures. Some major physical phenomena and experimental results of the mutual interactions between each crude oil and CO_2 are discussed in the subsequent sections.

Onset Pressure of Asphaltene Precipitation. For Joffre Viking light crude oil, the saturation pressure inside the saturation cell was increased from 3.0 MPa by 0.2 MPa in each step until the test pressure reached $P = 5.0$ MPa. It was found that, during the saturation test, the lower visual acrylic window was clean and transparent at $P < 5.0$ MPa, as shown in the first digital image in Figure 4a for $P = 3.0$ MPa. This means that there was no observable asphaltene precipitation. However, this figure shows that the digital image suddenly became dark at

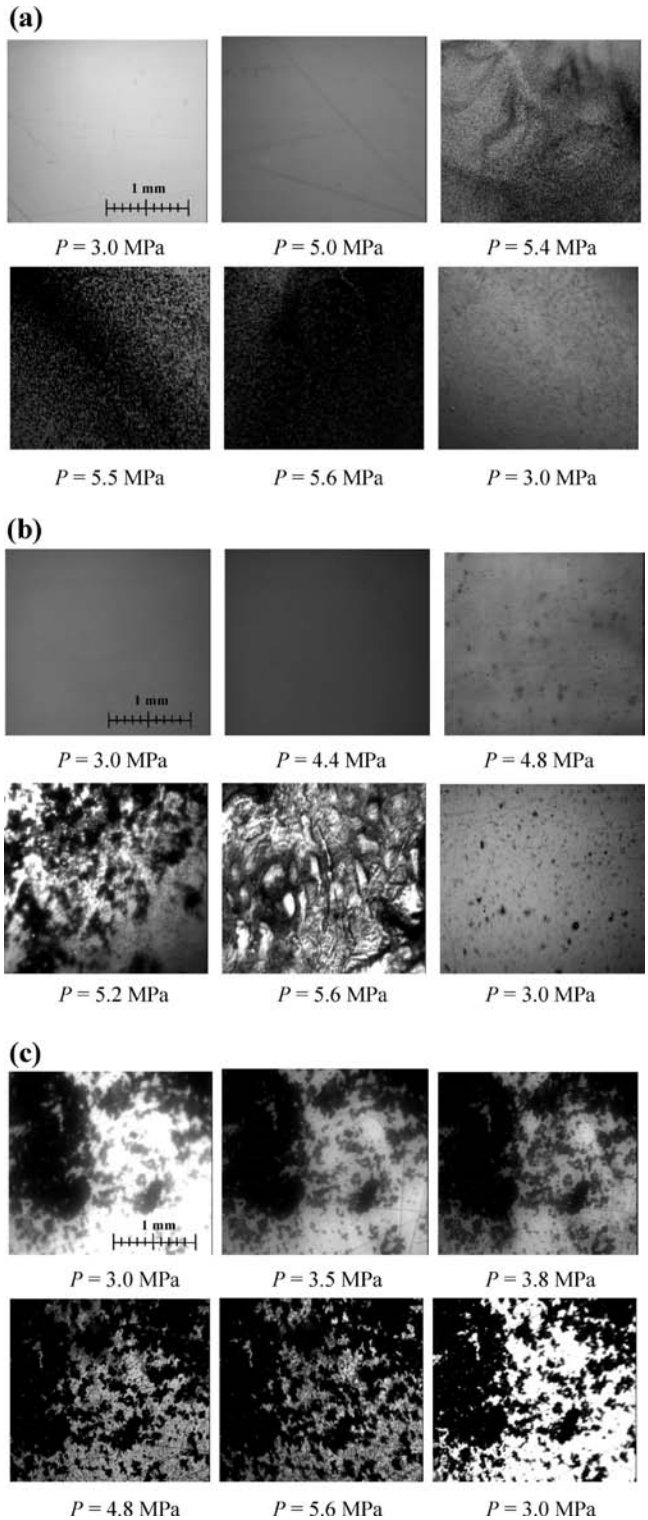

Figure 4. (a) Digital images of the asphaltenes precipitated from the Joffre Viking light crude oil−CO_2 system onto the lower acrylic window of the high-pressure saturation cell at various saturation pressures, 40× magnification, and $T = 300.15$ K. (b) Digital images of asphaltenes precipitated from the Pembina Cardium light crude oil−CO_2 system onto the lower acrylic window of the high-pressure saturation cell at various saturation pressures, 40 × magnification, and $T = 300.15$ K. (c) Digital images of the asphaltenes precipitated from the Weyburn medium crude oil−CO_2 system onto the lower acrylic window of the high-pressure saturation cell at various saturation pressures, 40× magnification, and $T = 300.15$ K.

$P = 5.0$ MPa, though the same light intensity was used. After this pressure, the saturation pressure was increased by 0.1 MPa in each step. At $P = 5.4$ MPa, some fine asphaltene particles were precipitated and observed in the CO_2-saturated oil layer. As the saturation pressure was further increased to $P = 5.5$ MPa, much more fine and dark asphaltene particles were observed, but they were separated from each other. Finally, at $P = 5.6$ MPa, an extremely large number of fine and dark asphaltene particles were precipitated. They remained separated from each other and were not coagulated into large deposits. At $P > 5.6$ MPa, the morphology of the precipitated asphaltene particles remained essentially unchanged with the saturation pressure.[14] It is concluded that the onset pressure of the asphaltene precipitation from CO_2-saturated Joffre Viking light crude oil tested in this study is $P_{asp} = 5.4$ MPa at $T = 300.15$ K. After the onset pressure of the asphaltene precipitation was determined, the saturation pressure was suddenly reduced to 3.0 MPa to ascertain the redissolution of the precipitated asphaltene particles or the reversibility of the asphaltene precipitation at a lower pressure. The last digital image in Figure 4a for $P = 3.0$ MPa shows that almost all the precipitated asphaltene particles were redissolved into the crude oil phase at this starting pressure. This observation shows that the asphaltene precipitation is almost reversible when the saturation pressure is suddenly reduced.[22]

For Pembina Cardium light crude oil, it was found that, at $P < 4.4$ MPa, there was no observable asphaltene precipitation, as shown in the first digital image in Figure 4b for $P = 3.0$ MPa. When the saturation pressure reached $P = 4.4$ MPa, the acquired digital image suddenly became dark at the same light intensity. Then the saturation pressure was increased by 0.1 MPa in each step. At $P = 4.8$ MPa, some precipitated asphaltene particles were observed in the CO_2-saturated oil layer. As the saturation pressure was further increased, the observed asphaltene deposits were large and dark. In this case, more asphaltene particles were precipitated and coagulated, as shown in this figure for $P = 5.2$ MPa. At $P = 5.6$ MPa, the precipitated asphaltene particles formed some larger deposits in a CO_2-saturated oil layer. At $P > 5.6$ MPa, the morphology of the precipitated asphaltene deposits remained almost unchanged with the saturation pressure. Therefore, the onset pressure of the asphaltene precipitation in CO_2-saturated Pembina Cardium light crude oil tested in this study is $P_{asp} = 4.8$ MPa at $T = 300.15$ K. After the saturation pressure was suddenly reduced to 3.0 MPa, almost all the precipitated asphaltene deposits were redissolved into the crude oil phase at this starting pressure, as shown in the last digital image in Figure 4b for $P = 3.0$ MPa.

For Weyburn medium crude oil, some black areas shown in the first digital image in Figure 4c for $P = 3.0$ MPa represented the thick oil layers, rather than the precipitated asphaltenes. The clean and transparent areas for the thin oil layers at $P = 3.0$ MPa were used to observe the asphaltene precipitation as the saturation pressure was increased by 0.1 MPa in each step. It was found that, at the saturation pressure of $P = 3.5$ MPa, the acquired digital image suddenly became dark at the same light intensity. At $P = 3.8$ MPa, some precipitated asphaltene particles were observed to move into the thin oil layers. As the pressure was increased to $P = 4.8$ MPa, more and more fine and dark asphaltene particles were observed, but they were separated from each other. Finally, at $P = 5.6$ MPa, a large number of asphaltene particles were precipitated. At $P > 5.6$ MPa, the morphology of the precipitated asphaltene particles remained almost unchanged. Hence, the onset pressure of the asphaltene precipitation in CO_2-saturated Weyburn medium crude oil tested in this study is determined to be $P_{asp} = 3.8$ MPa at $T = 300.15$ K. Afterward, the saturation pressure was suddenly reduced to 3.0 MPa. Most precipitated asphaltene particles were redissolved

Table 2. Four Measured Onset Pressures for Three Different Crude Oil−CO_2 Systems Tested at $T = 300.15$ K[a]

oilfield	Joffre Viking	Pembina Cardium	Weyburn
P_{asp}/MPa	5.4	4.8	3.8
P_{ext}/MPa	5.5	6.4	7.2
MMP/MPa	7.3 to 7.4	7.5 to 7.6	9.3
P_{max}/MPa	10.0	13.0	18.2

[a] P_{asp}: onset pressure of the asphaltene precipitation. P_{ext}: onset pressure of the initial strong light-components extraction. MMP: minimum miscibility pressure determined by applying the VIT technique. P_{max}: miscibility pressure between the heavy components of the original crude oil and CO_2, which is close to the so-called first-contact miscibility pressure.

into the crude oil phase at this starting pressure, as seen in the last digital image in Figure 4c for $P = 3.0$ MPa.

Table 2 shows the onset pressures of the asphaltene precipitation for the three crude oil−CO_2 systems. It is found that the onset pressure of the asphaltene precipitation for a crude oil−CO_2 system is lower if the asphaltene content of the crude oil is higher. Moreover, as Pembina Cardium light crude oil is obtained in the early CO_2 EOR stage, most asphaltenes of this light crude oil may not have precipitated and deposited onto the reservoir formations. Thus, a large number of asphaltene particles were precipitated and also aggregated to form some large deposits due to some coprecipitated resins,[5,23] as shown in Figure 4b for $P =$ (5.2 or 5.6) MPa. On the other hand, as Joffre Viking and Weyburn crude oils are collected in the intermediate CO_2 EOR stage, most asphaltenes and some resins of the crude oils may have coprecipitated and then codeposited onto the reservoir formations. Hence, the precipitated asphaltene particles were fine and did not further form large deposits, as seen from Figures 4a and 4c. Finally, the asphaltene precipitation from the three crude oil−CO_2 systems is found to be highly reversible when the saturation pressure is suddenly reduced.

Equilibrium IFT and MMP. For Joffre Viking light crude oil, the measured equilibrium IFTs between the crude oil and CO_2 at different equilibrium pressures of $P =$ (2.4 to 9.3) MPa and a constant temperature of $T = 300.15$ K are plotted in Figure 5a. It is found that the measured equilibrium IFT is reduced almost linearly with the equilibrium pressure in three distinct pressure ranges. In Range I [$P =$ (2.4 to 4.6) MPa], the equilibrium IFT reduction is attributed to the increased solubility or dissolution of CO_2 in the crude oil at an increased equilibrium pressure. In Range II [$P =$ (5.0 to 6.4) MPa], the equilibrium IFT was suddenly increased to a higher value at $P = 5.0$ MPa and then reduced quickly and linearly again as the equilibrium pressure was increased to $P = 6.4$ MPa. This is due to the asphaltene precipitation (at $P > P_{asp} = 5.4$ MPa) and initial strong light-components extraction (at $P > P_{ext} = 5.5$ MPa) from the original Joffre Viking light crude oil to the CO_2 phase in this pressure range.[14,21] As a result, the measured equilibrium IFT is between the relatively heavy components of the original light crude oil and CO_2. In Range III [$P =$ (6.4 to 9.3) MPa], even stronger light-components extraction was observed at the beginning of each IFT test. It should be noted that, in this pressure range, the measured equilibrium IFT is between even heavier components of the original light crude oil and CO_2. The equilibrium IFT was reduced slightly, and finally it reached its lowest value of $\gamma_{eq} = 1.16$ mJ·m^{-2} at the equilibrium pressure of $P = 9.3$ MPa.

On the basis of the measured data (symbols) in Figure 5a, the equilibrium IFT γ_{eq} is correlated to the equilibrium pressure P by applying the linear regression in the above-described three equilibrium pressure ranges, respectively

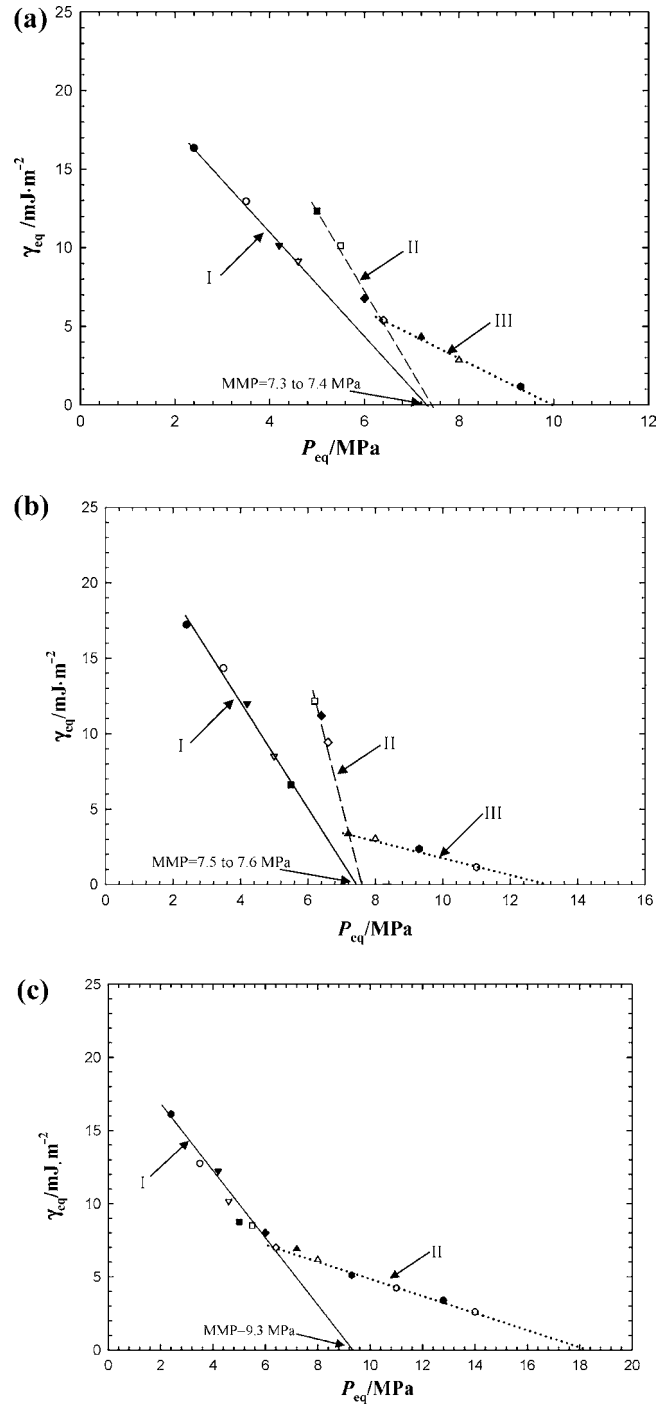

Figure 5. (a) Measured equilibrium interfacial tensions, γ_{eq}, of the Joffre Viking light crude oil−CO_2 system at different equilibrium pressures, P_{eq}, and $T = 300.15$ K. ●, $P = 2.4$ MPa; ○, $P = 3.5$ MPa; ▼, $P = 4.2$ MPa; ▽, $P = 4.6$ MPa; ■, $P = 5.0$ MPa; □, $P = 5.5$ MPa; ◆, $P = 6.0$ MPa; ◇, $P = 6.4$ MPa; ▲, $P = 7.2$ MPa; △, $P = 8.0$ MPa; ●, $P = 9.3$ MPa. Line I is eq 1; line II is eq 2; and line III is eq 3. (b) Measured equilibrium interfacial tensions, γ_{eq}, of the Pembina Cardium light crude oil−CO_2 system at different equilibrium pressures, P_{eq}, and $T = 300.15$ K. ●, $P = 2.4$ MPa; ○, $P = 3.5$ MPa; ▼, $P = 4.2$ MPa; ▽, $P = 5.0$ MPa; ■, $P = 5.5$ MPa; □, $P = 6.2$ MPa; ◆, $P = 6.4$ MPa; ◇, $P = 6.6$ MPa; ▲, $P = 7.2$ MPa; △, $P = 8.0$ MPa; ⬢, $P = 9.3$ MPa; ⬡, $P = 11.0$ MPa. Line I is eq 4; line II is eq 5; and line III is eq 6. (c) Measured equilibrium interfacial tensions, γ_{eq}, of the Weyburn medium crude oil−CO_2 system at different equilibrium pressures, P_{eq}, and $T = 300.15$ K. ●, $P = 2.4$ MPa; ○, $P = 3.5$ MPa; ▼, $P = 4.2$ MPa; ▽, $P = 4.6$ MPa; ■, $P = 5.0$ MPa; □, $P = 5.5$ MPa; ◆, $P = 6.0$ MPa; ◇, $P = 6.4$ MPa; ▲, $P = 7.2$ MPa; △, $P = 8.0$ MPa; ⬢, $P = 9.3$ MPa; ⬡, $P = 11.0$ MPa; ●, $P = 12.8$ MPa; ○, $P = 14.0$ MPa. Line I is eq 7; and line II is eq 8.

$$\gamma_{eq}/mJ\cdot m^{-2} = -3.35(P/MPa) + 24.45 \quad (2.4 \le P/MPa \le 4.6, R^2 = 0.996) \quad (1)$$

$$\gamma_{eq}/mJ\cdot m^{-2} = -5.18(P/MPa) + 38.30 \quad (5.0 \le P/MPa \le 6.4, R^2 = 0.988) \quad (2)$$

$$\gamma_{eq}/mJ\cdot m^{-2} = -1.48(P/MPa) + 14.86 \quad (6.4 \le P/MPa \le 9.3, R^2 = 0.995) \quad (3)$$

For the Joffre Viking light crude oil−CO_2 system, the respective linear regression equations of the measured equilibrium IFT versus equilibrium pressure data for Ranges I and II converge to almost the same equilibrium pressure (i.e., the MMP) at $\gamma_{eq} = 0$. The MMP of this system is determined by applying the VIT technique to be (7.3 to 7.4) MPa. On the other hand, the intersecting point of Range III and the abscissa, i.e., $P_{max} =$ 10.0 MPa, can be considered as the miscibility pressure between the heavy components of this light crude oil and CO_2, which is close to the so-called first-contact miscibility pressure.

For Pembina Cardium light crude oil, the measured equilibrium IFTs between the crude oil and CO_2 at different equilibrium pressures of $P =$ (2.4 to 11.0) MPa and a constant temperature of $T = 300.15$ K are plotted in Figure 5b. It is found that the measured equilibrium IFT is reduced almost linearly with the equilibrium pressure in the following three distinct pressure ranges: Range I [$P =$ (2.4 to 5.5) MPa], Range II [$P =$ (6.2 to 7.2) MPa], and Range III [$P =$ (7.2 to 11.0) MPa]. The equilibrium IFT is reduced slightly, and finally it reaches its lowest value of $\gamma_{eq} = 1.15$ mJ·m^{-2} at the equilibrium pressure of $P = 11.0$ MPa. In addition, the strong light-components extraction was observed at the beginning of each IFT test at $P \ge 6.4$ MPa.

On the basis of the measured data (symbols) in Figure 5b, the equilibrium IFT γ_{eq} is correlated to the equilibrium pressure P by applying the linear regression in the above-mentioned three pressure ranges, respectively

$$\gamma_{eq}/mJ\cdot m^{-2} = -3.47(P/MPa) + 26.03 \quad (2.4 \le P/MPa \le 5.5, R^2 = 0.988) \quad (4)$$

$$\gamma_{eq}/mJ\cdot m^{-2} = -9.06(P/MPa) + 68.84 \quad (6.2 \le P/MPa \le 7.2, R^2 = 0.987) \quad (5)$$

$$\gamma_{eq}/mJ\cdot m^{-2} = -0.59(P/MPa) + 7.68 \quad (7.2 \le P/MPa \le 11.0, R^2 = 0.988) \quad (6)$$

For the Pembina Cardium light crude oil−CO_2 system, the respective linear regression equations of the measured equilibrium IFT versus equilibrium pressure data for Ranges I and II converge to almost the same equilibrium pressure at $\gamma_{eq} = 0$, i.e., MMP = (7.5 to 7.6) MPa. Also, the miscibility pressure between the heavy components of this light crude oil and CO_2 is located at the intersection of Range III and the abscissa, i.e., $P_{max} = 13.0$ MPa.

For the Weyburn medium crude oil, the measured equilibrium IFTs between the crude oil and CO_2 at different equilibrium pressures of $P =$ (2.4 to 14.0) MPa and a constant temperature of $T = 300.15$ K are shown in Figure 5c. It is found that the measured equilibrium IFT is reduced almost linearly with the equilibrium pressure in two rather different pressure ranges: Range I [$P =$ (2.4 to 6.4) MPa] and Range II [$P =$ (6.4 to 14.0) MPa]. The equilibrium IFT reduces slightly and finally reaches $\gamma_{eq} = 2.60$ mJ·m^{-2} at the equilibrium pressure of $P =$ 14.0 MPa. As Weyburn medium crude oil has the least amount of light components, a sudden increase of the measured equilibrium IFT does not occur for this medium crude oil−CO_2 system. Relatively strong light-components extraction was observed at the beginning of each IFT test at $P \ge 7.2$ MPa.

On the basis of the measured data (symbols) in Figure 5c, the equilibrium IFT γ_{eq} is correlated to the equilibrium pressure P by applying the linear regression in the above-mentioned two pressure ranges, respectively

$$\gamma_{eq}/mJ\cdot m^{-2} = -2.26(P/MPa) + 21.04 \quad (2.4 \le P/MPa \le 6.4, R^2 = 0.961) \quad (7)$$

$$\gamma_{eq}/mJ\cdot m^{-2} = -0.60(P/MPa) + 10.90 \quad (6.4 \le P/MPa \le 14.0, R^2 = 0.990) \quad (8)$$

For the Weyburn medium crude oil−CO_2 system, the linear regression equation of the measured equilibrium IFT versus equilibrium pressure data for Range I intersects with the abscissa (i.e., $\gamma_{eq} = 0$) at $P = 9.3$ MPa at 300.15 K. Therefore, the MMP of this system is determined to be 9.3 MPa. In addition, the miscibility pressure between the heavy components of this medium crude oil and CO_2 is found to be $P_{max} = 18.2$ MPa from the linear regression equation for Range II.

Oil-Swelling Effect and Light-Components Extraction. It was observed in the IFT measurements that after the pendant oil drop was formed and surrounded by the CO_2 phase inside the high-pressure cell, its volume and shape were changed continuously. The onset pressures of the initial strong light-components extraction, P_{ext}, for these three crude oil samples are listed in Table 2. It is found that a heavier crude oil has a higher P_{ext}.

At a low equilibrium pressure ($P < P_{ext}$), the pendant oil drop first swelled slightly due to CO_2 dissolution into the oil phase and then shrank slowly because of the subsequent weak light-components extraction. The sequential digital images of the dynamic pendant oil drops and their volumes for the three different crude oil samples at $P = 3.5$ MPa and $T = 300.15$ K are shown in Figure 6a at four different times, $t = 0$ s, 30 s, 60 s, and 1000 s. It is clearly seen from this figure that the oil drop volume was increased slightly at the beginning ($t \le 30$ s) due to the initial oil-swelling effect. Afterward, the oil drop volume was reduced appreciably as a result of the subsequent weak light-components extraction from the oil phase to the CO_2 phase. This indicates that the oil-swelling effect due to CO_2 dissolution into the oil phase is more pronounced at the beginning ($t \le 30$ s), whereas the oil-shrinking effect due to light-components extraction becomes dominant at a large time (e.g., $t > 30$ s).[14,21]

At a high equilibrium pressure ($P \ge P_{ext}$), the strong light-components extraction was observed at the beginning and then followed by the subsequent weak light-components extraction. The sequential digital images of the dynamic pendant oil drops and their volumes for the three different crude oil samples at $P = 7.2$ MPa and $T = 300.15$ K are shown in Figure 6b at four different times, $t = 0$ s, 30 s, 100 s, and 1000 s. At the high pressure, the light components of each crude oil were rapidly

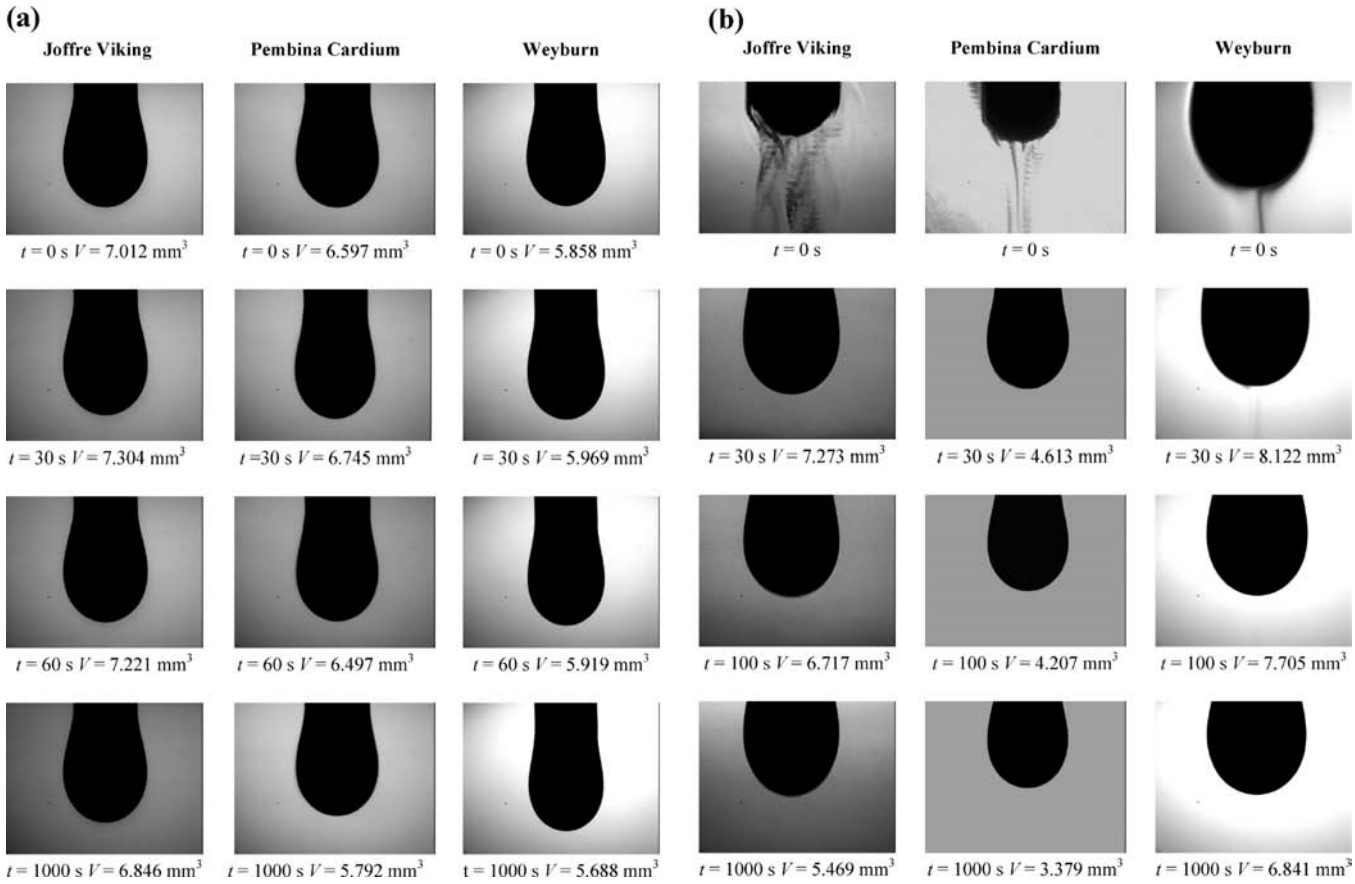

Figure 6. (a) Sequential digital images of pendant drops of three different crude oils surrounded by CO_2 at $P = 3.5$ MPa during the initial oil-swelling process ($0 \leq t/s \leq 30$) and the subsequent weak light-components extraction process ($30 \leq t/s \leq 1000$). (b) Sequential digital images of pendant drops of three different crude oils surrounded by CO_2 at $P = 7.2$ MPa during the initial strong light-components extraction process ($0 \leq t/s \leq 30$) and the subsequent weak light-components extraction process ($30 \leq t/s \leq 1000$).

extracted from the oil phase to the CO_2 phase at the beginning ($t \leq 30$ s). The initial strong light-components extraction greatly accelerated the vaporization of the light hydrocarbons. Then the pendant oil drop kept shrinking slowly due to the subsequent weak light-components extraction ($t > 30$ s). It should be mentioned that, in this case, the final well-shaped pendant oil drop is primarily composed of the remaining heavy components, which have rather different physicochemical properties from those of the original crude oil. This fact indicates that, at a high equilibrium pressure, the light-components extraction occurs at the beginning, and the oil properties change dramatically.[14,21] The light-components extraction from the oil phase to the CO_2 phase is always a dominant physical phenomenon at $P \geq P_{ext}$.

Conclusions

In this paper, three different crude oil−CO_2 systems are tested in a see-through windowed high-pressure saturation cell to determine their respective onset pressures (P_{asp}) of the asphaltene precipitation. It is found that the onset pressure of the asphaltene precipitation is lower if the asphaltene content of the crude oil is higher. The morphology of the asphaltenes precipitated from a crude oil strongly depends on CO_2 EOR stage. The measured equilibrium IFT is found to reduce almost linearly with the equilibrium pressure in three distinct pressure ranges for the two light crude oil−CO_2 systems and in two different pressure ranges for the medium crude oil−CO_2 system. The determined MMP is much higher if the crude oil is heavier. In addition, it is observed during the IFT measurements that if the test pressure is lower than the onset pressure of the initial strong light-components extraction (i.e., $P < P_{ext}$) the oil-swelling effect occurs after the crude oil contacts CO_2, and then the oil drop shrinks slowly. On the other hand, the initial strong light-components extraction is observed at $P \geq P_{ext}$ and then is followed by the subsequent weak light-components extraction. In summary, at $P \geq P_{asp}$, a crude oil is deasphalted, and thus its composition is considerably lighter due to CO_2 dissolution and asphaltene precipitation. Furthermore, at a higher pressure ($P \geq P_{ext}$), the initial strong light-components extraction significantly changes the compositions of both the oil and CO_2 phases. In this way, the multicontact miscibility between the crude oil and CO_2 is gradually developed and finally achieved at the MMP. At an even higher pressure ($P \approx P_{max}$), the miscibility between the heavy components of the original crude oil and CO_2, which is close to the so-called first-contact miscibility, can be reached ultimately.

Literature Cited

(1) Moritis, G. Special Report: EOR/Heavy Oil Survey. *Oil Gas J.* **2006**, *104*, 37–57.
(2) Farouq Ali, S. M.; Thomas, S. The Promise and Problems of Enhanced Oil Recovery Methods. *J. Can. Pet. Technol.* **1996**, *35*, 57–63.
(3) Pyo, K.; Damian-Diaz, N.; Powell, M.; van Nieuwkerk, J. CO_2 Flooding in Joffre Viking Pool. Paper 2003−109, *Proceeding of the 4th Canadian International Petroleum Conference*, Calgary, Alberta, 2003.
(4) Aycaguer, A. C.; Lev-On, M.; Winer, A. M. Reducing Carbon Dioxide Emissions with Enhanced Oil Recovery Projects: A Life Cycle Assessment Approach. *Energy Fuels* **2001**, *15*, 303–308.
(5) Srivastava, R. K.; Huang, S. S.; Dong, M. Asphaltene Deposition during CO_2 Flooding. *SPE Prod. Facil.* **1999**, *14*, 235–245.

(6) Brons, G.; Yu, J. M. Solvent Deasphalting Effects on Whole Cold Lake Bitumen. *Energy Fuels* **1995**, *9*, 641–647.
(7) Mansoori, G. A.; Vazquez, D.; Shariaty-Niassar, M. Polydispersity of Heavy Organics in Crude Oils and Their Role in Oil Well Fouling. *Fluid Phase Equilib.* **2006**, *58*, 375–390.
(8) Yang, D.; Tontiwachwuthikul, P.; Gu, Y. Interfacial Tensions of the Crude Oil + Reservoir Brine + CO_2 Systems at Pressures up to 31 MPa and Temperatures of 27 °C and 58 °C. *J. Chem. Eng. Data* **2005**, *50*, 1242–1249.
(9) Green, D. W.; Willhite, G. P. *Enhanced Oil Recovery*; SPE Textbook Series, SPE: Richardson, TX, 1998; Vol. 6.
(10) Hol, L. W.; Josendal, V. A. Mechanisms of Oil Displacement by Carbon Dioxide. *J. Pet. Technol.* **1974**, *26*, 1427–1438.
(11) Dong, M.; Huang, S. S.; Dyer, S. B.; Mourits, F. M. A Comparison of CO_2 Minimum Miscibility Pressure Determinations for Weyburn Crude Oil. *J. Pet. Sci. Eng.* **2001**, *31*, 13–22.
(12) Rao, D. N.; Lee, J. I. Application of the New Vanishing Interfacial Tension Technique to Evaluate Miscibility Conditions for the Terra Nova Offshore Project. *J. Pet. Sci. Eng.* **2002**, *35*, 247–262.
(13) Rao, D. N.; Lee, J. I. Determination of Gas-Oil Miscibility Conditions by Interfacial Tension Measurements. *J. Colloid Interface Sci.* **2003**, *262*, 474–482.
(14) Nobakht, M.; Moghadam, S.; Gu, Y. Determination of CO_2 Minimum Miscibility Pressure from the Measured and Predicted Equilibrium Interfacial Tensions. *Ind. Eng. Chem. Res.* **2008**, *47*, 8918–8925.
(15) Nobakht, M.; Moghadam, S.; Gu, Y. Mutual Interactions between Crude Oil and CO_2 under Different Pressures. *Fluid Phase Equilib.* **2008**, *265*, 94–103.
(16) ASTM D2007-03, Standard Test Method for Characteristic Groups in Rubber Extender and Processing Oils and Other Petroleum-Derived Oils by the Clay-Gel Absorption Chromatographic Method, 2003.
(17) Peng, D. Y.; Robinson, D. B. A New Two-constant Equation of State. *Ind. Eng. Chem. Fundam.* **1976**, *15*, 58–64.
(18) ASTM D86, Standard Test Method for Distillation of Petroleum Products at Atmospheric Pressure, 2009.
(19) Cheng, P.; Li, D.; Boruvka, L.; Rotenberg, Y.; Neumann, A. W. Automation of Axisymmetric Drop Shape Analysis for Measurements of Interfacial Tensions and Contact Angles. *Colloids Surf.* **1990**, *43*, 151–167.
(20) Yang, C.; Gu, Y. A New Experimental Method for Measuring Gas Diffusivity in Heavy Oil by the Dynamic Pendant Drop Volume Analysis (DPDVA). *Ind. Eng. Chem. Res.* **2005**, *44*, 4474–4483.
(21) Yang, D.; Gu, Y. Interfacial Interactions between Crude Oil and CO_2 under Reservoir Conditions. *Pet. Sci. Technol.* **2005**, *23*, 1099–1112.
(22) Hirschberg, A.; Dejong, L. N.; Schipper, B. A.; Meijer, J. G. Influence of Temperature and Pressure on Asphaltene Flocculation. *SPE J.* **1984**, *24*, 283–293.
(23) Mullins, O. C.; Sheu, E. Y. *Structures and Dynamics of Asphaltenes*; Plenum Press: New York, 1998.

Received for review May 27, 2010. Accepted August 13, 2010. The authors want to acknowledge the discovery grant from the Natural Sciences and Engineering Research Council (NSERC) of Canada and the innovation fund from the Petroleum Technology Research Centre (PTRC) at the University of Regina to Y. Gu.

JE1005664